Multiple twinning and variant-variant transformations in martensite: Phase-field approach

Valery I. Levitas,[1,*] Arunabha M. Roy,[2] and Dean L. Preston[3]

[1]*Departments of Mechanical Engineering, Aerospace Engineering, and Material Science and Engineering, Iowa State University, Ames, Iowa 50011, USA*

[2]*Department of Aerospace Engineering, Iowa State University, Ames, Iowa 50011, USA*

[3]*Computational Physics Division, Los Alamos National Laboratory, Los Alamos, New Mexico 87545, USA*

(Received 2 November 2012; revised manuscript received 12 August 2013; published 30 August 2013)

A phase-field theory of transformations between martensitic variants and multiple twinning within martensitic variants is developed for large strains and lattice rotations. It resolves numerous existing problems. The model, which involves just one order parameter for the description of each variant-variant transformation and multiple twinnings within each martensitic variant, allows one to prescribe the twin interface energy and width, and to introduce interface stresses consistent with the sharp interface limit. A finite-element approach is developed and applied to the solution of a number of examples of twinning and combined austenite-martensite and martensite-martensite phase transformations (PTs) and nanostructure evolution. A similar approach can be developed for reconstructive, electric, and magnetic PTs.

DOI: 10.1103/PhysRevB.88.054113 PACS number(s): 64.60.Bd, 63.70.+h, 64.60.an, 64.70.−p

I. INTRODUCTION

Twinning is a mechanism for plastic deformation in crystalline materials whereby a region of the crystal lattice is homogeneously sheared into a new orientation.[1] It is most pronounced at low temperatures, high strain rates, and in small grains. Martensitic phase transformations (PTs) are usually accompanied by twinning, which reduces the energy associated with internal elastic stresses. Martensitic PTs involve several martensitic variants M_i, $i = 1,2,\ldots,n$, where n equals the ratio of the order of the point group of the austenite A to that of the martensite. Since the M_i are usually in a twin relation to each other, variant-variant transformations and twinning in martensite are closely related. The sharp-interface approach to martensitic PTs and twinning[2,3] was a significant advance, but it is based on the optimization of crystallographic parameters of the prescribed microstructure under stress-free conditions or applied homogeneous stresses. The phase-field approach is widely used for modeling microstructure evolution during multivariant martensitic PTs and twinning.[4–8] Phase-field models that incorporate the main features of stress-strain curves, the correct instability conditions, a large strain formulation, and surface tension were developed in Refs. 7 and 9–12; those models utilize order parameters based on the transformation strain. Since it was shown in Ref. 9 that it is not possible to realize all of these model features using total-strain order parameters, we will only consider order parameters based on transformation strain. In this paper, we present a phase-field model for variant-variant transformations and multiple twinning within the martensite, which resolves numerous problems outlined below. It also includes $\mathsf{A} \leftrightarrow \mathsf{M}_i$ PTs. For each twinning system $\{\mathsf{T}_1,\mathsf{T}_2,\ldots,\mathsf{T}_n\}$, where the T_i are crystallographically equivalent, the transformation-deformation gradient $\boldsymbol{F}_{ti} = \boldsymbol{I} + \gamma(\eta_i)\boldsymbol{m}_i^0 \otimes \boldsymbol{n}_i^0$ transforms the parent (reference) lattice L into a twinned lattice T_i by a simple shear γ in direction $\boldsymbol{m}_i^0$ in the plane with normal $\boldsymbol{n}_i^0$ in the reference state; here η_i, the ith order parameter, varies between 0 for L and 1 for T_i, $\otimes$ designates a dyadic product of vectors, and $\boldsymbol{I}$ is the unit tensor. It is usually assumed that twinning can be described by a phase-field model of PT for which the thermal part of the free energy does not change and the transformation strain corresponds to the twinning shear.[7–9] However, this is not completely consistent because of an essential difference between twinning and PTs: twinning does not change the crystal structure, i.e., the unit cell of the twin is the same as that of the parent crystal to within a rigid-body rotation. This fact introduces a symmetry requirement not present in the PT theory: the thermodynamic potential and the transformation-deformation gradient must be completely symmetric with respect to the interchange $\mathsf{L} \leftrightarrow \mathsf{T}_i$; thus, any twin T_i can be considered as a parent reference lattice L. Our 2-3-4 Landau potential for martensitic PT[9,10] possesses this symmetry, but our 2-4-6 potential[9,10] does not. However, the main theoretical complication is multiple twinning, that is, secondary and further twinnings of the primary twin T_i, which commonly occurs. Again, since the crystal lattice of any twin T_i is indistinguishable to within rigid-body rotations from the parent lattice L, the thermodynamic potential and transformation-deformation gradient must be completely symmetric with respect to the interchanges $\mathsf{L} \leftrightarrow \mathsf{T}_i$ and $\mathsf{T}_j \leftrightarrow \mathsf{T}_i$ for all i and j. This condition was not satisfied in any previous model of PTs and twinning but is satisfied in the present model for twinning in martensite. The crystal lattice of the austenite A will be considered as the parent (reference) lattice, independent of whether we consider PT $\mathsf{A} \leftrightarrow \mathsf{M}_i$ or only $\mathsf{M}_i \leftrightarrow \mathsf{M}_j$. Below, we will no longer consider designation L, and designations M_i and T_i are equivalent.

Even for small strains, neither transformations between martensitic variants nor twinning in any known theory is described as consistently as $\mathsf{A} \leftrightarrow \mathsf{T}_i$ transformations. Indeed, the $\mathsf{A} \leftrightarrow \mathsf{T}_i$ transformation can be described by a single order parameter η_i, the temperature dependence of the stress-strain curve, and the A-T_i interface energy and width are completely determined by a small number of material parameters, and we obtained analytic solutions for the variation of η_i through both static and propagating interfaces.[10,12,13] In contrast, at a T_i-T_j interface in any known theory, the order parameters η_i and η_j vary independently, and the transformation path in the η_i-η_j plane and the interface energy and width have

an unrealistic dependence on temperature, stresses, and a larger number of material parameters; these dependencies can only be determined by numerical methods.[11] Thus, one cannot prescribe a desired T_i-T_j interface energy and width. Consequently, the consistency of the expression introduced in Refs. 11 and 12 for the interface (surface) tension $\boldsymbol{\sigma}_{\rm st}$ in the sharp-interface limit can be proved for A-T_i interfaces but not for T_i-T_j interfaces; in fact, simulations show that $\boldsymbol{\sigma}_{\rm st}$ does not describe the sharp T_i-T_j interface limit. This shortcoming is rectified in the model presented here. Also, in large strain theory,[7,8] in which each martensitic variant or twin is characterized by the transformation deformation gradient $\boldsymbol{F}_{ti}$, the transformations $\mathsf{T}_i \leftrightarrow \mathsf{T}_j$ between $\boldsymbol{F}_{ti}$ and $\boldsymbol{F}_{tj}$ do not represent simple shears without additional rotations. There are an infinite number of combinations of rotations and twinning parameters for which two martensitic variants are twin-related, e.g., zigzag twins.[3] Thus, it is impossible to parametrize all simple shears between two martensitic variants with a single order parameter.

In this paper, we present a phase-field model of martensitic variant-variant ($\mathsf{T}_i \leftrightarrow \mathsf{T}_j$) transformations and twinning within the variants which resolves all of the above problems. Each martensitic variant is characterized by the rotation-free deformation of the crystal lattice $\boldsymbol{U}_{ti}$. We define a minimal set of n order parameters for n martensitic variants. The key point is that each $\mathsf{T}_i \leftrightarrow \mathsf{T}_j$ transformation and all twinnings within them are described with a single order parameter. This significantly simplifies the description of $\mathsf{T}_i \leftrightarrow \mathsf{T}_j$ transformations and multiple twinnings, and moreover, one can prescribe the T_i-T_j interface energy and width and introduce interface stresses consistent with the sharp interface approach, which is completely analogous to the description of $\mathsf{A} \leftrightarrow \mathsf{T}_i$ PT. For the fully geometrically nonlinear theory (large strains and material rotation), the twinning parameters and lattice rotations are not parametrized with the order parameters but obtained from the solution of the coupled phase field and mechanics boundary-value problem. Model problems on twinning in martensite and combined $\mathsf{A} \leftrightarrow \mathsf{T}_i$ and $\mathsf{T}_j \leftrightarrow \mathsf{T}_i$ transformations and nanostructure evolution in a nanosize sample are solved by means of the finite-element method (FEM) COMSOL code.[14]

We designate contractions of tensors $\boldsymbol{A} = \{A_{ij}\}$ and $\boldsymbol{B} = \{B_{ji}\}$ over one and two indices as $\boldsymbol{A}\cdot\boldsymbol{B} = \{A_{ij}\,B_{jk}\}$ and $\boldsymbol{A}\!:\!\boldsymbol{B} = A_{ij}\,B_{ji}$, respectively. The subscripts s, e, and t mean symmetrization and elastic and transformational strains, the superscript T designates transposition, and ∇ is the gradient operator in the *deformed* states.

II. GENERAL MODEL

The motion of the elastic material undergoing twinning will be described by a vector-valued function $\boldsymbol{r} = \boldsymbol{r}(\boldsymbol{r}_0,t)$, where $\boldsymbol{r}_0$ and $\boldsymbol{r}$ are the positions of points in the reference Ω_0 and the deformed Ω configurations, respectively, and t is the time. The austenite A lattice will be considered as the reference configuration, independent of whether we consider PT $\mathsf{A} \leftrightarrow \mathsf{T}_i$ or only $\mathsf{T}_i \leftrightarrow \mathsf{T}_j$ transformations. The transformation deformation gradient $\boldsymbol{U}_{ti} = \boldsymbol{I} + \boldsymbol{\varepsilon}_{ti}$ transforms the crystal lattice of A into the lattice of the ith martensitic variant T_i, $i = 1,2,\ldots,n$, both in the unloaded state. The multiplicative decomposition of the deformation gradient, $\boldsymbol{F} = \boldsymbol{F}_e\cdot\boldsymbol{U}_t$, into elastic $\boldsymbol{F}_e$ and transformational $\boldsymbol{U}_t$ parts will be used. Since $\boldsymbol{U}_t = \boldsymbol{U}_t^T$, lattice rotation is included in $\boldsymbol{F}_e$. We assume the martensitic variants are in twin relation with each other, hence they satisfy the twinning equation $\boldsymbol{Q}_i\cdot\boldsymbol{U}_{ti} - \boldsymbol{Q}_j\cdot\boldsymbol{U}_{tj} = \gamma_{ij}\,\boldsymbol{m}_{ij}^0\boldsymbol{n}_{ij}^0$ for some twinning system parameters γ_{ij}, $\boldsymbol{m}_{ij}^0$, $\boldsymbol{n}_{ij}^0$, and rigid-body rotations $\boldsymbol{Q}_m$. There are numerous solutions to the twinning equation for the same $\boldsymbol{U}_{ti}$ and $\boldsymbol{U}_{tj}$ and different $\boldsymbol{Q}_m$. For example, for zigzag twins,[3] if each of the pairs of variants $\{\boldsymbol{R}\cdot\boldsymbol{U}_{ti};\boldsymbol{U}_{tj}\}$ and $\{\boldsymbol{Q}\cdot\boldsymbol{U}_{tj};\boldsymbol{R}\cdot\boldsymbol{U}_{ti}\}$ satisfies the twinning equations for some specific rotations $\boldsymbol{R}$ and $\boldsymbol{Q}$, then the pair of variants $\{\boldsymbol{Q}^p\cdot\boldsymbol{R}\cdot\boldsymbol{U}_{ti};\boldsymbol{Q}^p\cdot\boldsymbol{U}_{tj}\}$ satisfies the twinning equations as well for any integer number p of sequential rotations $\boldsymbol{Q}$. Thus, it is impractical (and unnecessary) to parametrize all *simple shears* between all pairs of martensitic variants with a separate order parameter. Instead, we describe martensitic variant T_i with the rotation-free transformation deformation gradient $\boldsymbol{U}_{ti}$, and all possible twinnings and variant-variant transformations between two variants will be described with a single order parameter. The twinning system parameters are not functions of the order parameters but are determined via the solution of the coupled large-strain phase field and mechanics boundary-value problem.

In our n-dimensional order parameter space, the austenite A is located at the origin and the ith martensitic variant T_i is located at the intersection of the positive ith axis with the unit sphere. The radial coordinate, designated $\boldsymbol{\Upsilon}$, describes $\mathsf{A} \leftrightarrow \mathsf{T}_i$ transformations, while the angular order parameters $0 \leqslant \vartheta_i \leqslant 1$, where $\pi\,\vartheta_i/2$ is the angle between the radius vector $\boldsymbol{\Upsilon}$ and the positive ith axis, describe twinning $\mathsf{T}_k \leftrightarrow \mathsf{T}_i$ (variant-variant) transformations. This geometric interpretation leads to the constraint $\sum_{k=1}^n \cos^2(\frac{\pi}{2}\vartheta_k) = 1$, which significantly complicates the development of the thermodynamic potential. However, for each variant-variant or twinning transformation $\mathsf{T}_i \leftrightarrow \mathsf{T}_j$ (at $\Upsilon = 1$, $\vartheta_k = 1$ for $k \neq i, j$), this constraint reduces to the linear constraint $\vartheta_j + \vartheta_i = 1$. In the general case, we also employ a linear constraint: $\sum_{i=1}^n \vartheta_i = n - 1$. This slightly changes the geometric interpretation when more than two order parameters ϑ_i deviate from 1, but it allows us to develop a potential that predicts both A-T_i and T_i-T_j interface widths and energies. Then $\vartheta_n = n - 1 - \sum_{i=1}^{n-1}\vartheta_i$ replaces all occurrences of the parameter ϑ_n in all equations below. The Helmholtz free energy per unit undeformed volume is given by the following expression:

$$\psi = \psi^e(\boldsymbol{B},\Upsilon,\vartheta_i,\theta) + \frac{\rho_0}{\rho}\check{\psi}^\theta + \psi^\theta + \frac{\rho_0}{\rho}\psi^\nabla, \tag{1}$$

$$\begin{aligned}\check{\psi}^\theta = {}& [A_0(\theta-\theta_c) + 3\Delta s_0(\theta-\theta_e)]\Upsilon^2(1-\Upsilon)^2 \\ & + \bar{A}\sum_{i,j=1;i\neq j}^{n}(1-\vartheta_i)^2(1-\vartheta_j)^2 q(\Upsilon) \\ & + D\sum_{i,j,k=1;i\neq j\neq k}^{n}(1-\vartheta_i)(1-\vartheta_j)(1-\vartheta_k)q(\Upsilon),\end{aligned} \tag{2}$$

$$\psi^\nabla = \frac{\beta}{2}|\nabla\Upsilon|^2 + q(\Upsilon)\frac{\beta_\vartheta}{4}\sum_{i=1}^{n}|\nabla\vartheta_i|^2,$$

$$\psi^\theta = -\Delta s_0(\theta-\theta_e)q(\Upsilon), \quad q(\Upsilon) = \Upsilon^2(3-2\Upsilon), \tag{3}$$

$$\boldsymbol{U}_t = \boldsymbol{I} + \sum_{k=1}^{n} \boldsymbol{\varepsilon}_{tk}\left(1 - 3\vartheta_k^2 + 2\vartheta_k^3\right)\varphi(\Upsilon),$$
$$\varphi(\Upsilon) = a\Upsilon^2 + (4-2a)\Upsilon^3 + (a-3)\Upsilon^4. \tag{4}$$

Here $\boldsymbol{B} = (\boldsymbol{V}\cdot\boldsymbol{V} - \boldsymbol{I})/2$ is the finite strain measure, $\boldsymbol{V}$ is the left stretch tensor, θ is the temperature, θ_e is the equilibrium temperature, A becomes unstable at temperature θ_c, ρ and ρ_0 are the mass densities in the deformed and undeformed states, β and β_ϑ are gradient energy coefficients, A_0 and $\bar{A}$ characterize the barriers for A-T_i and T_i-T_j transformations, respectively, the parameter a controls the transformation strain for A-T_i PT, and ψ^e is the elastic energy. The term with D in Eq. (2) describes the interaction of three twins at their triple junctions; it was not present in previous theories and it disappears for two variants. Thermodynamics and Landau-Ginzburg kinetics (see, e.g., Ref. 11) lead to

$$\boldsymbol{\sigma} = \frac{\rho}{\rho_0}\boldsymbol{V}\cdot\frac{\partial\psi}{\partial\boldsymbol{B}}\cdot\boldsymbol{V} - \frac{\rho}{\rho_0}\left(\nabla\Upsilon\otimes\frac{\partial\psi}{\partial\nabla\Upsilon}\right)_s - \sum_{i=1}^{n-1}\frac{\rho}{\rho_0}\left(\nabla\vartheta_i\otimes\frac{\partial\psi}{\partial\nabla\vartheta_i}\right)_s, \tag{5}$$

$$\frac{1}{L_\Upsilon}\frac{\partial\Upsilon}{\partial t} = -\frac{\rho}{\rho_0}\frac{\partial\psi}{\partial\Upsilon}\bigg|_{\boldsymbol{B}} + \nabla\cdot\left(\frac{\rho}{\rho_0}\frac{\partial\psi}{\partial\nabla\Upsilon}\right),$$
$$\frac{1}{L_\vartheta}\frac{\partial\vartheta_i}{\partial t} = -\frac{\rho}{\rho_0}\frac{\partial\psi}{\partial\vartheta_i}\bigg|_{\boldsymbol{B}} + \nabla\cdot\left(\frac{\rho}{\rho_0}\frac{\partial\psi}{\partial\nabla\vartheta_i}\right), \tag{6}$$

where L_Υ and L_ϑ are kinetic coefficients, $\boldsymbol{\sigma}$ is the true Cauchy stress tensor, and $\partial\psi/\partial\Upsilon$ and $\partial\psi/\partial\vartheta_i$ are evaluated at constant finite strain $\boldsymbol{B}$. Equations (1)–(4) satisfy all conditions for the thermodynamic potential formulated in Ref. 9. In particular, A and the variants T_i are homogeneous solutions of the Ginzburg-Landau equations (6) for arbitrary stresses and temperature; the transformation strain for any transformation is independent of stresses and temperature; the transformation criteria that follow from the thermodynamic instability conditions have the same (correct) form as in Ref. 9. The potential (1)–(4) is much simpler than those previously used for martensitic PTs[7,9–11] and does not require the introduction of sophisticated cross terms, which has several important consequences. In particular, the potential does not possess spurious minima (unphysical phases). All of our modeling goals are satisfied using a simple fourth-degree polynomial in Υ and ϑ_i. The variant-variant or twinning transformations $\mathsf{T}_i \leftrightarrow \mathsf{T}_j$ are described by a single order parameter ϑ_i (at $\Upsilon = 1$, $\vartheta_k = 1$ for $k \neq i, j$, and $\vartheta_j = 1 - \vartheta_i$) and are completely analogous to A $\leftrightarrow \mathsf{T}_i$ PTs. The ratio ρ_0/ρ and the gradient with respect to the deformed configuration are used in Eqs. (1)–(4) to introduce interface tension, as in Refs. 11 and 12. Since the $\mathsf{T}_j \leftrightarrow \mathsf{T}_i$ transformations are described here in the same way as A $\leftrightarrow \mathsf{T}_i$ PT, it is now trivial to demonstrate (see Sec. III) the consistency of the expression for the interface tension [obtained from Eq. (5) after subtracting the elastically supported stress] with the sharp interface limit, whereas this could be proved only for A-T_i interfaces in Ref. 12. The thermodynamic potential and $\boldsymbol{U}_t$ are symmetric with respect to the interchanges $\mathsf{T}_j \leftrightarrow \mathsf{T}_i$; they need not be symmetric with respect to the interchange A $\leftrightarrow \mathsf{T}_i$ because A $\leftrightarrow \mathsf{T}_i$ is not a twinning.

III. EQUIVALENCE OF EQUATIONS FOR L-T_k AND T_i-T_j TRANSFORMATIONS

Let us simplify Eqs. (2)–(6) for the austenite-martensite phase transformation by setting $\vartheta_2 = 0$, $\vartheta_i = 1$ for $i \neq 2$. We also set $a = 3$, which leads to $\varphi(\Upsilon) = q(\Upsilon)$. This is necessary to make the transformation strain between the austenite and martensite symmetric with respect to the interchanges A $\leftrightarrow \mathsf{T}_i$, in the same sense as it is symmetric for variant-variant transformation. Then

$$\breve{\psi}^\theta = [A_0(\theta-\theta_c) + 3\Delta s_0(\theta-\theta_e)]\Upsilon^2(1-\Upsilon)^2, \tag{7}$$

$$\psi^\nabla = \frac{\beta}{2}|\nabla\Upsilon|^2, \tag{8}$$

$$\boldsymbol{U}_t = \boldsymbol{I} + \boldsymbol{\varepsilon}_{t2}q(\Upsilon), \tag{9}$$

$$\boldsymbol{\sigma} = \frac{\rho}{\rho_0}\boldsymbol{V}\cdot\frac{\partial\psi}{\partial\boldsymbol{B}}\cdot\boldsymbol{V} - \frac{\rho}{\rho_0}\left(\nabla\Upsilon\otimes\frac{\partial\psi}{\partial\nabla\Upsilon}\right)_s, \tag{10}$$

$$\frac{1}{L_\Upsilon}\frac{\partial\Upsilon}{\partial t} = -\frac{\rho}{\rho_0}\frac{\partial\psi}{\partial\Upsilon}\bigg|_{\boldsymbol{B}} + \nabla\cdot\left(\frac{\rho}{\rho_0}\frac{\partial\psi}{\partial\nabla\Upsilon}\right). \tag{11}$$

Next, let us simplify Eqs. (2)–(6) for the $\mathsf{T}_1 \leftrightarrow \mathsf{T}_2$ transformation but setting $\Upsilon = 1$, $\vartheta = \vartheta_1$, $\vartheta_2 = 1 - \vartheta$, and $\vartheta_i = 1$ for $2 < i \leqslant n$. Then

$$\breve{\psi}^\theta = \bar{A}\vartheta^2(1-\vartheta)^2, \tag{12}$$

$$\psi^\nabla = \frac{\beta_\vartheta}{2}|\nabla\vartheta|^2, \tag{13}$$

$$\boldsymbol{U}_t = \boldsymbol{I} + \boldsymbol{\varepsilon}_{t1} + (\boldsymbol{\varepsilon}_{t2} - \boldsymbol{\varepsilon}_{t1})q(\vartheta), \tag{14}$$

$$\boldsymbol{\sigma} = \frac{\rho}{\rho_0}\boldsymbol{V}\cdot\frac{\partial\psi}{\partial\boldsymbol{B}}\cdot\boldsymbol{V} - \frac{\rho}{\rho_0}\left(\nabla\vartheta\otimes\frac{\partial\psi}{\partial\nabla\vartheta}\right)_s, \tag{15}$$

$$\frac{1}{L_\vartheta}\frac{\partial\vartheta}{\partial t} = -\frac{\rho}{\rho_0}\frac{\partial\psi}{\partial\vartheta}\bigg|_{\boldsymbol{B}} + \nabla\cdot\left(\frac{\rho}{\rho_0}\frac{\partial\psi}{\partial\nabla\vartheta}\right). \tag{16}$$

It is clear that Eqs. (7)–(11) are equivalent to Eqs. (12)–(16) after substituting $\Upsilon \leftrightarrow \vartheta$ with the following correspondence of parameters:

$$[A_0(\theta-\theta_c) + 3\Delta s_0(\theta-\theta_e)] \leftrightarrow \bar{A},$$
$$\beta \leftrightarrow \beta_\vartheta, \quad \boldsymbol{\varepsilon}_{t1} \leftrightarrow 0, \quad L_\Upsilon \leftrightarrow L_\vartheta. \tag{17}$$

For the austenite-martensite interface, the combination of Eq. (1) and Eqs. (7)–(11) resulted in the desired expression for the interface (surface) tension $\boldsymbol{\sigma}_{\rm st}$.[11,12] Since Eqs. (12)–(16) for twinning are equivalent to Eqs. (7)–(11) for the austenite-martensite transformation, the expression for the interface tension $\boldsymbol{\sigma}_{\rm st}$ for the T_i-T_j interface has the same desired expression. This proves the advantage of the chosen order parameters and phase-field formulation in comparison with previous studies. Note that for the particular case considered in simulations, $A_0 = -3\Delta s_0$, the term $[A_0(\theta-\theta_c) + 3\Delta s_0(\theta-\theta_e)] = A_0(\theta_e - \theta_c)$ is temperature-independent.

IV. ANALYTICAL SOLUTIONS

An analytical solution for a nonequilibrium plane austenite-martensite interface moving in an infinite medium in the x

direction under stress-free conditions ($\psi^e = 0$) is[10,12]

$$\begin{aligned}\Upsilon &= 1/\left[1+e^{-p(x-v_\Upsilon t)/\delta_\Upsilon}\right],\\ \delta_\Upsilon &= p\sqrt{\beta/\{2[A_0(\theta-\theta_c)+3\Delta s_0(\theta-\theta_e)]\}},\\ v_\Upsilon &= -6L_\Upsilon\delta_\Upsilon\Delta s_0(\theta-\theta_e)/p,\\ E_\Upsilon &= \sqrt{2\beta[A_0(\theta-\theta_c)+3\Delta s_0(\theta-\theta_e)]}/6,\end{aligned} \tag{18}$$

where $p = 2.667$,[10] and v_Υ, δ_Υ, and E_Υ are the interface velocity, width, and energy, respectively. Using the above equivalence, similar equations can be obtained for a stationary variant-variant interface (since stresses are absent):

$$\begin{aligned}\vartheta &= 1/\left[1+e^{-p(x-v_\vartheta t)/\delta_\vartheta}\right], \quad \delta_\vartheta = p\sqrt{\beta_\vartheta/(2\bar{A})},\\ E_\vartheta &= \sqrt{2\beta_\vartheta\bar{A}}/6.\end{aligned} \tag{19}$$

These equations allow us to calibrate material parameters β, A_0, $\bar{A}$, and L when the temperature dependence of the interface energy, width, and velocity is known. An explicit expression for a variant-variant interface energy allows us to correctly define interface stresses at a variant-variant interface.

V. COMPLETE SYSTEM OF EQUATIONS FOR TWO MARTENSITIC VARIANTS

Below we enumerate the total system of equations for two martensitic variants used in our simulations. Elastic strains are considered to be small, which simplifies the equations significantly. Transformation strains and rotations are finite.

Kinematic decomposition:

$$\begin{aligned}\boldsymbol{F} &= \boldsymbol{F}_e\cdot\boldsymbol{U}_t, \quad \boldsymbol{F}_e = \boldsymbol{V}_e\cdot\boldsymbol{R}_e,\\ \boldsymbol{V}_e &= \boldsymbol{I}+\boldsymbol{\varepsilon}_e, \quad \boldsymbol{\varepsilon}_e \ll \boldsymbol{I},\end{aligned} \tag{20}$$

where $\boldsymbol{V}_e$ is the elastic left stretch tensor, $\boldsymbol{R}_e$ is the lattice rotation, and $\boldsymbol{\varepsilon}_e$ is the small elastic strains.

Transformation deformation gradient ($\vartheta = \vartheta_1$, $\vartheta_2 = 1-\vartheta$, and $a = 3$):

$$\boldsymbol{U}_t = \boldsymbol{I} + [\boldsymbol{\varepsilon}_{t1}(1-3\vartheta^2+2\vartheta^3)+\boldsymbol{\varepsilon}_{t2}(3\vartheta^2-2\vartheta^3)]q(\Upsilon). \tag{21}$$

The Helmholtz free energy per unit undeformed volume:

$$\psi = \psi^e + \frac{\rho_0}{\rho}\breve{\psi}^\theta + \psi^\theta + \frac{\rho_0}{\rho}\psi^\nabla, \tag{22}$$

$$\psi^e = \frac{1}{2}K\varepsilon_{0e}^2 + \mu\boldsymbol{e}_e:\boldsymbol{e}_e, \tag{23}$$

$$\breve{\psi}^\theta = A_0(\theta_e-\theta_c)\Upsilon^2(1-\Upsilon)^2 + \bar{A}(1-\vartheta)^2\vartheta^2 q(\Upsilon), \tag{24}$$

$$\psi^\nabla = \frac{\beta}{2}|\nabla\Upsilon|^2 + q(\Upsilon)\frac{\beta_\vartheta}{2}|\nabla\vartheta|^2, \tag{25}$$

$$\psi^\theta = -\Delta s_0(\theta-\theta_e)q(\Upsilon), \quad q(\Upsilon) = \Upsilon^2(3-2\Upsilon), \tag{26}$$

where ε_{0e} and $\boldsymbol{e}_e$ are the volumetric and deviatoric parts of the elastic strain tensor.

Decomposition of the Cauchy stress $\boldsymbol{\sigma}$ into elastic $\boldsymbol{\sigma}_e$ and surface tension $\boldsymbol{\sigma}_{st}$ tensors:

$$\begin{aligned}\boldsymbol{\sigma} &= \boldsymbol{\sigma}_e + \boldsymbol{\sigma}_{\rm st}; \qquad \boldsymbol{\sigma}_e = K\varepsilon_{0e}\boldsymbol{I} + 2\mu\boldsymbol{e}_e;\\ \boldsymbol{\sigma}_{\rm st} &= (\psi^\nabla + \breve{\psi}_\theta)\boldsymbol{I} - \beta_\Upsilon\nabla\Upsilon\otimes\nabla\Upsilon - q(\Upsilon)\beta_\vartheta\nabla\vartheta\otimes\nabla\vartheta.\end{aligned} \tag{27}$$

Ginzburg-Landau equations:

$$\begin{aligned}\frac{1}{L_\Upsilon}\frac{\partial\Upsilon}{\partial t} &= \boldsymbol{\sigma}_e{:}\left(\boldsymbol{R}_e\cdot\frac{\partial\boldsymbol{U}_t}{\partial\Upsilon}\cdot\boldsymbol{U}_t^{-1}\cdot\boldsymbol{R}_e^t\right)_s - \frac{\rho}{\rho_o}\frac{\partial\psi^\theta}{\partial\Upsilon} - \frac{\partial\breve{\psi}^\theta}{\partial\Upsilon} - \frac{\partial\psi^\nabla}{\partial\Upsilon} + \nabla\cdot\left(\frac{\partial\psi^\nabla}{\partial\nabla\Upsilon}\right)\\ &= \boldsymbol{\sigma}_e{:}\left(\boldsymbol{R}_e\cdot\frac{\partial\boldsymbol{U}_t}{\partial\Upsilon}\cdot\boldsymbol{U}_t^{-1}\cdot\boldsymbol{R}_e^t\right)_s + \frac{6\Delta s_0(\theta-\theta_e)}{1+\varepsilon_o}\Upsilon(1-\Upsilon) - 6\bar{A}\Upsilon(1-\Upsilon)\vartheta^2(1-\vartheta)^2\\ &\quad - 2A_0(\theta_e-\theta_c)\Upsilon(1-3\Upsilon+2\Upsilon^2) - 3\beta_\vartheta\Upsilon(1-\Upsilon)|\nabla\vartheta|^2 + \beta_\Upsilon\nabla^2\Upsilon,\end{aligned} \tag{28}$$

$$\begin{aligned}\frac{1}{L_\vartheta}\frac{\partial\vartheta}{\partial t} &= \boldsymbol{\sigma}_e{:}\left(\boldsymbol{R}_e\cdot\frac{\partial\boldsymbol{U}_t}{\partial\vartheta}\cdot\boldsymbol{U}_t^{-1}\cdot\boldsymbol{R}_e^t\right)_s - \frac{\partial\breve{\psi}^\theta}{\partial\vartheta} + \nabla\cdot\left(\frac{\partial\psi^\nabla}{\partial\nabla\vartheta}\right)\\ &= \boldsymbol{\sigma}_e{:}\left(\boldsymbol{R}_e\cdot\frac{\partial\boldsymbol{U}_t}{\partial\vartheta}\cdot\boldsymbol{U}_t^{-1}\cdot\boldsymbol{R}_e^t\right)_s - 2\bar{A}\vartheta q(\Upsilon)(1-3\vartheta+2\vartheta^2) + \beta_\vartheta q(\Upsilon)\nabla^2\vartheta.\end{aligned} \tag{29}$$

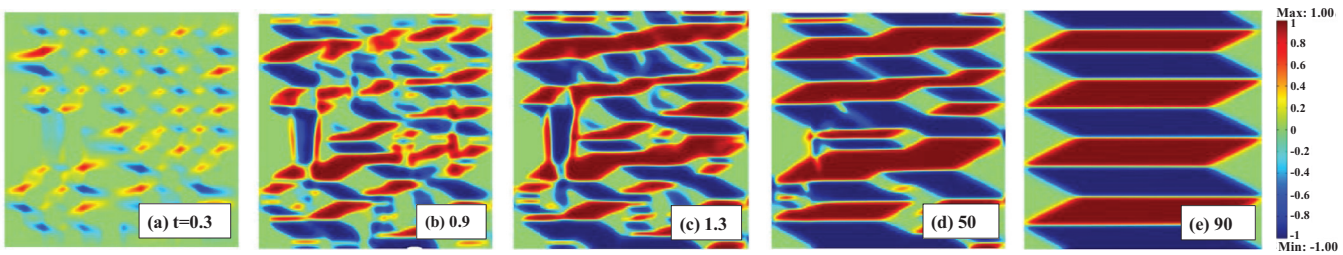

FIG. 1. (Color online) Evolution of $2\Upsilon(\vartheta-0.5)$ in a square sample of size 50×50 with an initial stochastic distribution of order parameter Υ under biaxial normal strain of 0.01.

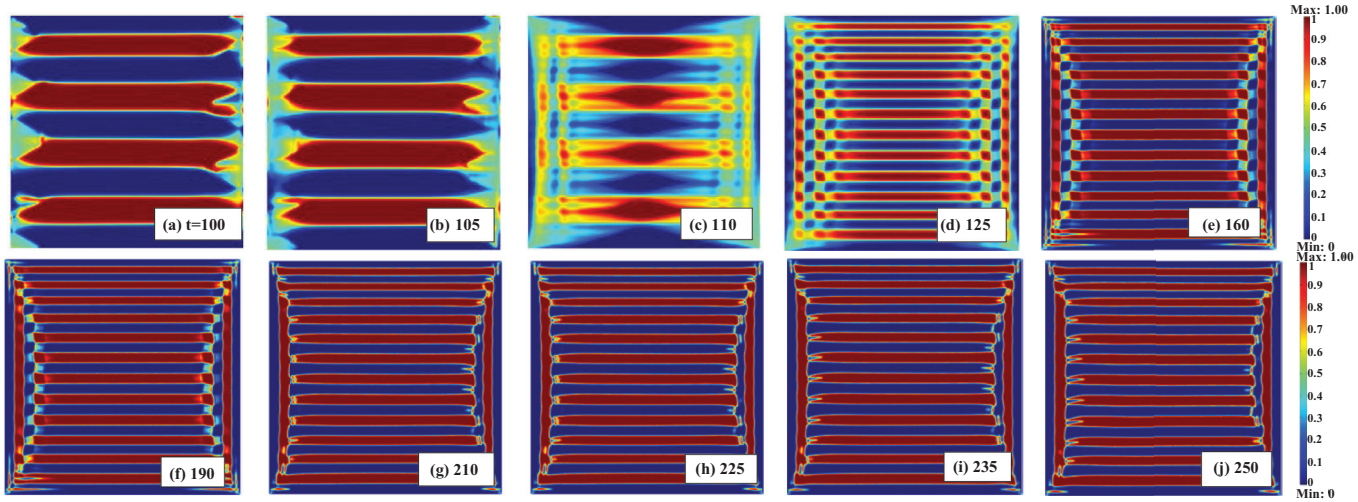

FIG. 2. (Color online) Evolution of ϑ in a square sample of size 50×50 under biaxial normal strain of 0.01 with an initial condition shown in Fig. 1(e), reduced temperature $\theta = 0$ K, parameter $\beta_\vartheta = 5.18 \times 10^{-11}$ N, and changed transformation strain.

Equilibrium equation:

$$\nabla \cdot \boldsymbol{\sigma} = \mathbf{0}. \tag{30}$$

In our example simulations, we use the material parameters for the cubic to tetragonal PT in NiAl found in Refs. 9, 10, and 13: $a = 3$, $A_0 = -3\Delta s_0 = 4.4$ MPa K^{-1}, $\bar{A} = 5320$ MPa, $\theta_c = -183$ K, $\theta_e = 215$ K, $L_\Upsilon = L_\vartheta = 2596.5$ m^2/N s, $\beta = \beta_\vartheta = 5.18 \times 10^{-10}$ N, and $\theta = 100$ K, unless stated otherwise. These parameters correspond to a twin interface energy $E_{\text{TT}} = 0.958$ J/m^2 and width $\Delta_{\text{TT}} = 0.832$ nm. Isotropic linear elasticity is used for simplicity; bulk modulus $K = 112.8$ GPa and shear modulus $\mu = 65.1$ GPa. In the plane stress two-dimensional (2D) problems, only T_1 and T_2 are considered; the corresponding transformation strains in the cubic axes are $\boldsymbol{\varepsilon}_{t1} = (0.215, -0.078, -0.078)$ and $\boldsymbol{\varepsilon}_{t2} = (-0.078, 0.215, -0.078)$. The FEM approach was developed and incorporated in the COMSOL code. All lengths, stresses, and times are given in units of nm, GPa, and ps. All external stresses are normal to the deformed surface.

VI. BENCHMARK PROBLEM: BENDING AND SPLITTING OF MARTENSITE TIPS IN NiAl ALLOYS

Our goal here is to reproduce several nontrivial microstructures observed in experiments for NiAl alloys.[15,16] Since numerous alternative solutions exist, one has to carefully choose initial conditions. We did this in several steps. The initial random distribution of order parameter Υ in the range $[0; 0.4]$ was prescribed in a square sample of 50×50 with the austenite lattice rotated by $\alpha = 45^\circ$. The initial value of ϑ was 0.5. For one horizontal and one vertical surface, the roller support was used, i.e., normal displacements and shear stresses are zero. Homogeneous normal displacements at two other surfaces were prescribed and kept constant during simulations, resulting in biaxial normal strain of 0.01. Shear stresses were kept zero at external surfaces. The two-dimensional problem under plane stress condition and temperature $\theta = 50$ K was studied. The evolution of $2\Upsilon(\vartheta - 0.5)$ is presented in Fig. 1, demonstrating transformation of the austenite into martensite and coalescence of martensitic units.

Despite the symmetry in geometry and boundary conditions, accidental asymmetry in the initial conditions led to the formation of an alternating horizontal martensitic twin structure with austenitic regions near vertical sides, in order to satisfy boundary conditions. Invariant plane conditions for the austenite-martensite interfaces are a consequence of a simplified plane-stress two-dimensional formulation.

The stationary solution from Fig. 1 was taken as an initial condition for the next problem with the following modifications: temperature was reduced to $\theta = 0$ K; parameter β_ϑ was reduced to $\beta_\vartheta = 5.18 \times 10^{-11}$ N, which led to twin interface energy $E_{\text{MM}} = 0.303$ J/m^2 and width $\Delta_{\text{MM}} = 0.263$ nm;

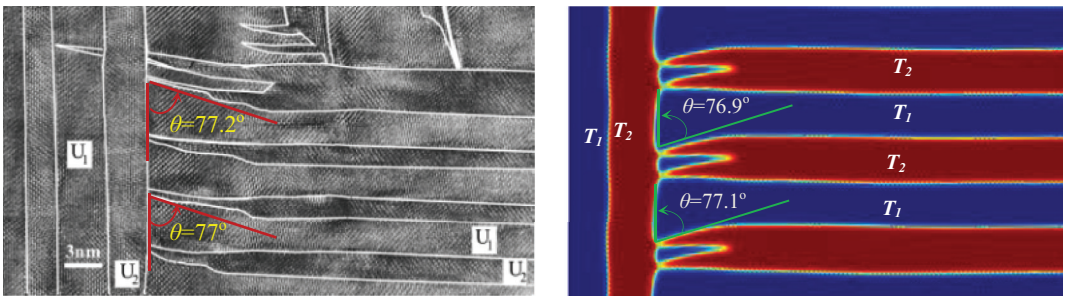

FIG. 3. (Color online) Comparison of transmission electron microscopy image of a nanostructure for NiAl alloy from Ref. 15 and the zoomed part of the simulation results from Fig. 2(j). Simulations reproduce well tip splitting and bending angle.

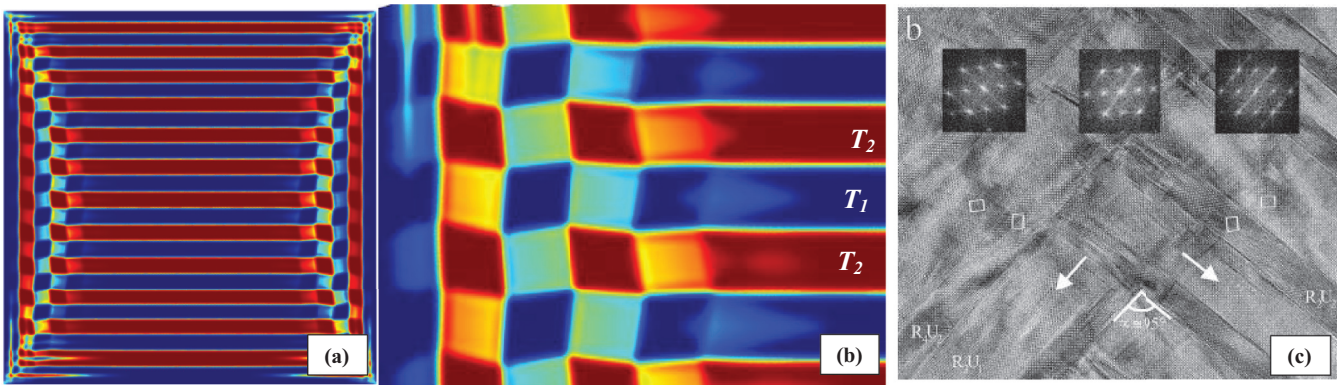

FIG. 4. (Color online) (a) Stationary solution for $2\Upsilon(\vartheta - 0.5)$ in a sample and (b) its zoomed part near the left side of a sample; (c) transmission electron microscopy of a nanostructure for NiAl from Ref. 15. Crossing twins are observed in experiment and simulation.

components of transformation strains have been changed to the values $\boldsymbol{U}_{t1} = (k_1,k_2,k_2)$ and $\boldsymbol{U}_{t2} = (k_2,k_1,k_2)$ with $k_1 = 1.15$ and $k_2 = 0.93$ corresponding to the NiAl alloy in Ref. 15. Then Υ was made equal to 1 everywhere and maintained during the entire simulation. Due to a reduction in the interface energy, the number of twins increased by splitting the initial twins (Fig. 2). Without austenite, rigid vertical boundaries led to high elastic energy. That is why restructuring produced vertical twins near each of the vertical sides in proportion, reducing the energy of the elastic stresses due to the prescribed horizontal strain. When the microstructure transforms to fully formed twins separated by diffuse interfaces, narrowing and bending of the tips of horizontal T_2 plates is observed (Figs. 2 and 3), similar to experiments.[15] Note that since the invariant plane interface between T_1 and T_2 requires mutual rotation of these variants by the angle $\omega = 12.1^\circ$ [$\cos\omega = 2k_1k_2/(k_1^2 + k_2^2) = 0.9778$],[15] the angle between the horizontal and vertical variants T_2 is $1.5\omega = 18.15^\circ$, which is in good agreement with our simulations. Thus, due to lattice rotations, the interface between the horizontal and vertical variants T_2 cannot be an invariant plane interface, and a reduction in the internal stresses at this boundary leads to a reduction of the boundary area by narrowing and bending of the tips of one horizontal plate. The measured angles between the tangent to the bent tip and the horizontal line in the experiment[15] and in calculations (Fig. 3) are in good quantitative agreement.

Note that microstructure evolution occurs through intermediate values of ϑ in some regions (see $t = 125$ and 160 in Fig. 2), i.e., when transformation strain of one twin penetrates into the region of another one, producing crossed twins. Such crossed twins have been observed in some experiments[16] and have been arrested (Fig. 4). In our simulations in Fig. 2, they represent an intermediate stage of evolution. However, if we reduce $\bar{A}$ to 0.532 GPa, such crossed twins represent stationary solutions (Fig. 4). Also, on the right side of the solution in Fig. 2, an alternative way for stress relaxation is visible, when twins T_2 are surrounded by twins T_1, which is also observed in experiments.[15]

Thus, starting with a microstructure in Fig. 1, which is quite far from the final one, our solution reproduced three types of nontrivial experimentally observed microstructures involving finite rotations, including tip splitting and bending, twins crossing, and good quantitative agreement for the bending angle. Note that tip splitting and bending were also reproduced in Ref. 5 utilizing strain-based phase-field formulation and initial conditions closer to the final solution than here.

VII. PHASE TRANSFORMATION AND TWINNING UNDER APPLIED LOAD

A. Nanoindentation: Applied uniform pressure

Nanoindentation-induced twinning $\mathsf{T}_2 \rightarrow \mathsf{T}_1$ was studied in a T_2 sample with a preexisting T_1 embryo of radius 2 under the indenter (Fig. 5). The sample was obtained from a square A sample of size 50×50 by transforming it homogeneously to T_2. The cubic axes and transformation strain were rotated by $\alpha = 31^\circ$ with respect to the coordinate axes. Initial conditions were as follows: $\Upsilon = 1$ everywhere, $\vartheta = 0.9$ inside the embryo, and $\vartheta = 0.999$ in the rest of the sample. A uniform pressure between the indenter of width 4 and the sample was increased linearly from 2 to 3 GPa over 110 ps. The bottom sample surface was constrained by a roller support and point F was fixed; all other surfaces are stress-free. With increasing

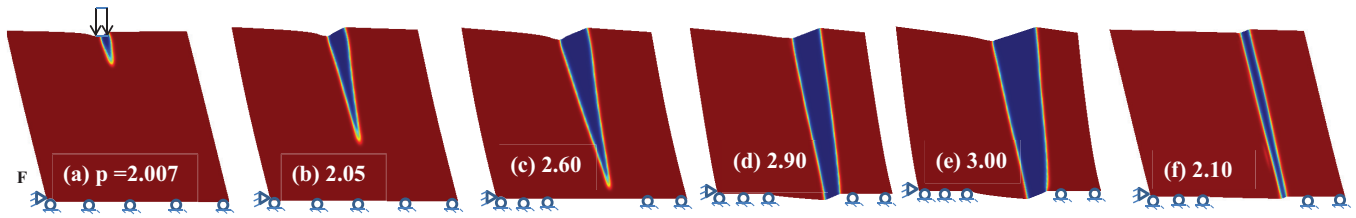

FIG. 5. (Color online) Twinning T_2 (red) $\rightarrow \mathsf{T}_1$ (blue) under indentation with the rigid support (a),(b), support with the hole (c)–(e), and during unloading (f).

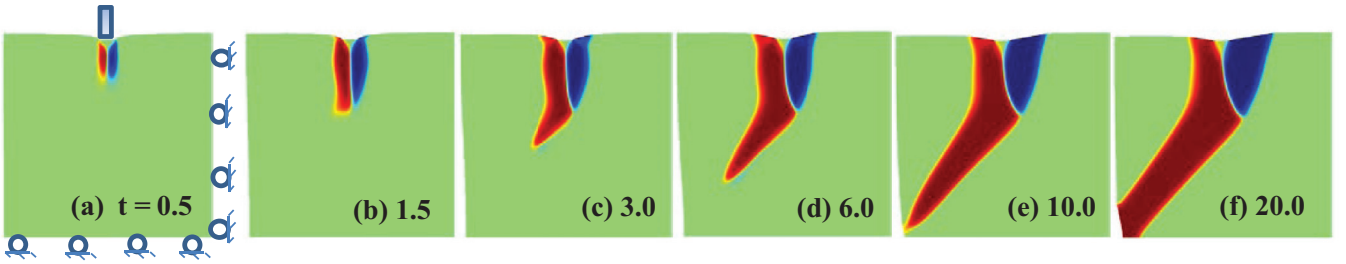

FIG. 6. (Color online) Evolution of $2\Upsilon(\vartheta - 0.5)$ for indentation of A (green) sample; T_2: red and T_1: blue.

load, a twin T_1 appears under the indenter and grows in a wedge shape with a sharp tip [Figs. 5(a) and 5(b)]. Since the bottom of the sample was constrained by the roller support, the twin T_1 could not propagate through the entire sample. In the same problem but with a stress-free section of length 20 at the bottom [Figs. 5(c) and 5(d)], the twin propagated completely through the sample and widened with increasing load. The load was then reduced to zero: the width of the twin then decreased to zero without a change in length [Figs. 5(e) and 5(f)]. These results are in qualitative agreement with experiments[1] and previous simulations.[8] Since dislocation plasticity and interface friction[6,13] are neglected, there is no residual twin.

B. Nanoindentation: Applied uniform displacement

Nanoindentation of a square 50×50 A sample with $\alpha = 15^\circ$ was modeled by prescribing uniform vertical displacements growing from 2 to 2.5 over a section of width 4; friction was neglected (Fig. 6). Adjacent lateral surfaces of the sample were constrained by the roller supports. In an initial embryo of radius 2, we set $\Upsilon = 0.1$; $\Upsilon = 0.01$ outside of the embryo. The order parameter $\vartheta = 0.5$ everywhere. The transformed twinned martensite first grew only in the vertical direction; note the presence of a small nontransformed region under the indenter [Figs. 6(a)–6(f)]. When the stress concentration due to the indenter became smaller than the internal stresses due to transformation strain and the bottom constraint, a morphological transition occurred: the growth of T_2 changed direction away from T_1 toward a corner of the sample, and ultimately reached the corner. The T_2-T_1 interface is curvilinear and consequently cannot be described by crystallographic theories presented in, e.g., Refs. 2 and 3.

C. Biaxial stresses

A square A sample of size 100×100 with $\alpha = 15^\circ$ and an embryo of 2 nm radius in the center of the sample was subjected to uniform vertical and horizontal stresses $\sigma_y = 3$ and $\sigma_x = 0.1$, respectively (Fig. 7). Because of the reflection symmetry, only one-quarter of the sample was directly simulated; roller supports were applied along the symmetry axes. The parameter values $\bar{A} = 61.6$ MPa and $\beta_{TT} = 19.4 \times 10^{-12}$ N were used, corresponding to $E_{TT} = 0.01$ J/m^2 and $\Delta_{TT} = 1$ nm. The initial conditions in the embryo were $\Upsilon = 0.1$, and $\Upsilon = 0.001$ outside the embryo; $\vartheta = 0.5$ everywhere. Within 1 ps, A was transformed to a mixture of T_i twins, which further evolve to produce a nontrivial stationary morphology. Note that varying the ratio L_ϑ / L_Υ from 1 to 1000 with $L_\Upsilon = 2596.5$ m^2/N s did not change the stationary solution and only slightly affected the evolution.

D. Double indentation

Two indenters of width 4 nm were placed on adjacent sides of a square 50×50 A sample with $\alpha = 45^\circ$ (Fig. 8). At $t = 0$, there were uniform pressures $p_1 = p_2 = 3$ across the indenters. The remaining lateral surfaces of the sample were constrained by roller supports. In two initial embryos of radius 2 under the indenters, $\Upsilon = 0.1$; outside the embryos, $\Upsilon = 0.01$. Again, $\vartheta = 0.5$ everywhere. The complex evolution of the twinned nanostructure is shown in Figs. 8(a)–8(i). Starting with state (h), p_2 was slowly reduced to zero while keeping $p_1 = 3$. The quasistationary solutions in Figs. 8(j)–8(l) show an initial reversal of the nanostructure [see Figs. 8(j) and 8(g)] followed by the predominance of T_1.

VIII. CONCLUDING REMARKS

To summarize, a phase-field model of transformations between martensitic variants and multiple twinning in martensitic variants was developed. It accounts for large strains and lattice rotations, and incorporates a minimal set of order parameters.

Each martensitic variant is characterized by the rotation-free deformation of the crystal lattice $\boldsymbol{U}_{ti}$. The twinning parameters and lattice rotations are not parametrized with the

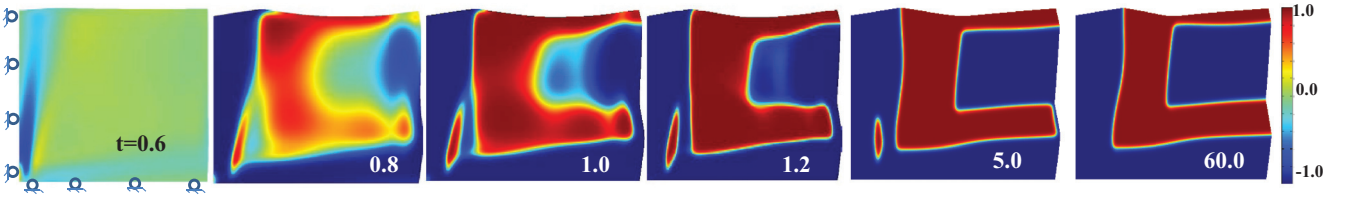

FIG. 7. (Color online) Evolution of $2\Upsilon(\vartheta - 0.5)$ in a quarter of 100×100 sample with an initial embryo at the center under homogeneous compressive stress of $\sigma_y = 3$ and $\sigma_x = 0.1$.

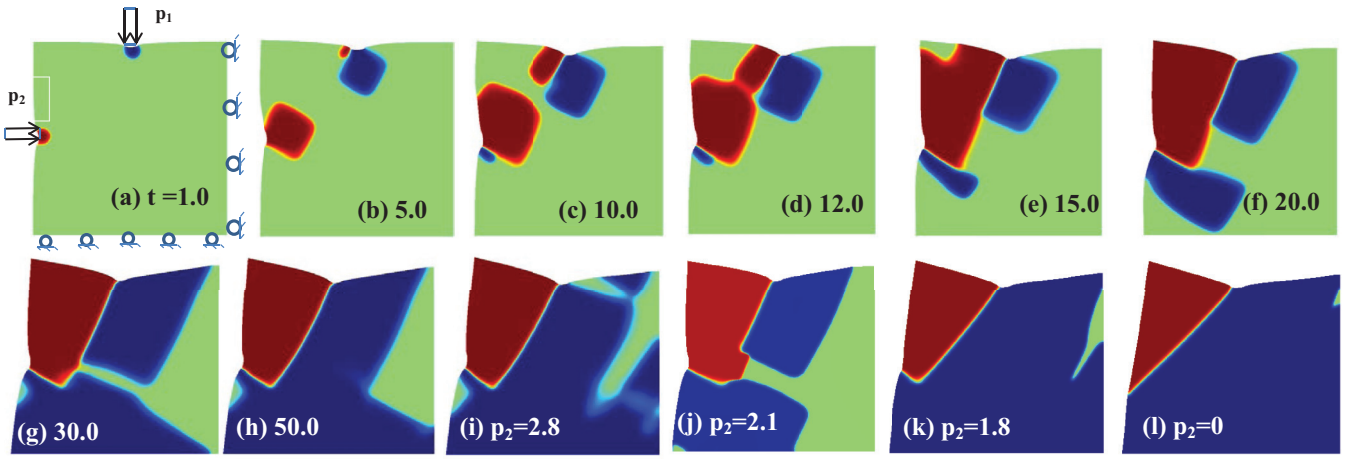

FIG. 8. (Color online) Evolution of $2\Upsilon(\vartheta - 0.5)$ in time (a)–(i) for double indentation of an A sample at $p_1 = p_2 = 3$, followed by reduction of p_2 to zero at $p_1 = 3$ (j)–(l) from state (h).

order parameters but are obtained from the solution of the coupled phase field and mechanics boundary-value problem. Each variant-variant transformation and all of the infinite number of possible twinnings within them are described with a single order parameter. Despite this economy of order parameters, arbitrarily complex twin-within-a-twin martensitic microstructures can in principle be described by the model. The energies and widths of the A-T_i and T_j-T_i interfaces can be controlled (prescribed), and the corresponding interface stresses are consistent with the sharp interface limit. A similar approach in terms of order parameters (Υ, ϑ_i) could be developed for reconstructive, electric, and magnetic PTs and for other phenomena described by multiple order parameters. Problems on twinning in martensite and combined A $\leftrightarrow$ M_i and $M_j \leftrightarrow M_i$ transformations and nanostructure evolution in a nanosize sample are solved utilizing the FEM. In particular, for thermally induced transformation, we reproduced three types of nontrivial experimentally observed microstructures involving finite rotations, including tip splitting and bending and twins crossing; good quantitative agreement for the bending angle is obtained.

ACKNOWLEDGMENT

The support of LANL (Contract No. 104321), Army Research Office (Grant No. W911NF-12-1-0340), National Science Foundation (Grant No. CMMI-0969143), DARPA (Grant No. W31P4Q-13-1-0010), Office of Naval Research (Grant No. N00014-12-1-0525), and ISU is gratefully acknowledged.

*vlevitas@iastate.edu

[1] J. W. Christian and S. Mahajan, Prog. Mater. Sci. **39**, 1157 (1995); V. S. Boiko, R. I. Garber, and A. M. Kosevich, *Reversible Crystal Plasticity* (AIP, New York, 1994).

[2] A. G. Khachaturyan and G. A. Shatalov, Sov. Phys. JETP **29**, 557561 (1969); A. L. Roitburd, Sov. Phys. Usp. **17**, 3255 (1974); J. M. Ball and R. D. James, Arch. Rat. Mech. Anal. **100**, 13 (1987); M. A. Grinfeld, *Thermodynamic Methods in the Theory of Heterogeneous Systems* (Longman, Sussex, 1991).

[3] K. Bhattacharya, *Microstructure of Martensite: Why It Forms and How It Gives Rise to the Shape-Memory Effect* (Oxford Series on Materials Modeling, 2003).

[4] T. W. Heoa, Y. Wang, S. Bhattacharya, X. Sun, S. Hu, and L. Q. Chen, Philos. Mag. Lett. **91**, 110 (2011); L. Q. Chen, Annu. Rev. Mater. Res. **32**, 113 (2002); A. Artemev, Y. Jin, and A. G. Khachaturyan, Acta Mater. **49**, 1165 (2001); M. Porta, T. Castán, P. Lloveras, T. Lookman, A. Saxena, and S. R. Shenoy, Phys. Rev. B **79**, 214117 (2009); O. U. Salman, B. K. Muite, and A. Finel, arXiv:1101.4748 (cond-mat.mtrl-sci); O. U. Salman, A. Finel, R. Delville, and D. Schryvers, J. Appl. Phys. **111**, 103517 (2012).

[5] A. Finel, Y. Le Bouar, A. Gaubert, and U. Salman, C. R. Phys. **11**, 245 (2010).

[6] V. I. Levitas and D.-W. Lee, Phys. Rev. Lett. **99**, 245701 (2007).

[7] V. I. Levitas and D. L. Preston, Phys. Lett. A **343**, 32 (2005); V. I. Levitas, V. A. Levin, K. M. Zingerman, and E. I. Freiman, Phys. Rev. Lett. **103**, 025702 (2009); V. I. Levitas, Int. J. Plasticity **49**, 85 (2013); V. A. Levin, V. I. Levitas, K. M. Zingerman, and E. I. Freiman, Int. J. Solids Struct. **50**, 2914 (2013).

[8] J. D. Clayton and J. Knap, Physica D **240**, 841 (2011); Model. Simul. Mater. Sci. Eng. **19**, 085005 (2011).

[9] V. I. Levitas and D. L. Preston, Phys. Rev. B **66**, 134206 (2002); **66**, 134207 (2002).

[10] V. I. Levitas, D. L. Preston, and D.-W. Lee, Phys. Rev. B **68**, 134201 (2003).

[11] V. I. Levitas and M. Javanbakht, Phys. Rev. Lett. **105**, 165701 (2010); Int. J. Mater. Res. **102**, 652 (2011).

[12] V. I. Levitas, Phys. Rev. B **87**, 054112 (2013); Acta Mater. **61**, 4305 (2013).

[13] V. I. Levitas, D.-W. Lee, and D. L. Preston, Int. J. Plast. **26**, 395 (2010).

[14] COMSOL, Inc., website: www.comsol.com.

[15] Ph. Boullay, D. Schryvers, R. V. Kohn, and J. M. Ball, J. Phys. IV **11**, 23 (2001); Ph. Boullay, D. Schryvers, and R. V. Kohn, Phys. Rev. B **64**, 144105 (2001).

[16] Ph. Boullaya, D. Schryvers, and J. M. Ball, Acta Mater. **51**, 1421 (2002).